HSV-1 infection induces a downstream-shift of +1 nucleosomes

Elena Weiß[1], Adam W. Whisnant[2,3], Thomas Hennig[2,3], Lara Djakovic[2], Lars Dölken[2,3,4#], Caroline C. Friedel[1#]

[1] Institute of Informatics, Ludwig-Maximilians-Universität München, Amalienstr. 17, 80333 Munich, Germany

[2] Institute for Virology and Immunobiology, Julius-Maximilians-University Würzburg, Versbacher Straße 7, 97078 Würzburg, Germany

[3] Institute for Virology, Medizinische Hochschule Hannover, Carl-Neuberg-Str. 1, 30625 Hannover, Germany

[4] Helmholtz Institute for RNA-based Infection Research (HIRI), Helmholtz-Center for Infection Research (HZI), 97080 Würzburg, Germany

[*] Corresponding authors

E-mail: lars.doelken@uni-wuerzburg.de; Caroline.Friedel@bio.ifi.lmu.de

Abstract

Herpes simplex virus 1 (HSV-1) infection induces a genome-wide loss of host transcriptional activity and widespread disruption of host transcription termination. The latter leads to read-through transcription for thousands of nucleotides beyond poly(A) sites and is associated with induction of open chromatin downstream of genes. In this study, we show that chromatin accessibility around promoters is also massively altered by HSV-1 infection as nucleosome-free regions around promoters are extended into regions downstream of transcription start sites, in particular for highly expressed genes. This was independent of HSV-1 immediate-early genes ICP0, ICP22, and ICP27 and the virion host shutoff protein *vhs*, but was reduced by treatment with phosphonoacetic acid (PAA), which inhibits viral DNA replication and alleviates the loss of RNA Polymerase II (Pol II) from host genes in HSV-1 infection. ChIPmentation analysis of the noncanonical histone variant H2A.Z, which is strongly enriched at +1 and -1 nucleosomes, indicated that the downstream extension of accessible chromatin at promoters was linked to a downstream shift of +1 nucleosomes. In yeast, downstream shifts of +1 nucleosomes can be induced by Pol II degradation. We confirmed that Pol II depletion is sufficient to similarly alter +1 nucleosome positioning in human cells by analyzing H2A.Z occupancy upon treatment with α-amanitin, which triggers degradation of the largest Pol II subunit. In summary, our study provides strong evidence that HSV-1-induced depletion of Pol II from the host genome leads to a widespread downstream shift of +1 nucleosomes at host gene promoters.

Author summary

Herpes simplex virus 1 (HSV-1) infection leads to a massive shutoff of host transcription. Loss of RNA Polymerase II (Pol II) in yeast has previously been shown to lead to a relaxation of +1 nucleosome positioning to more thermodynamically favorable sites downstream of transcription start sites. In this study, we show that a similar phenomenon is likely also at play in HSV-1 infection as sequencing of accessible chromatin reveals a widening of nucleosome-free regions at promoters into downstream regions. By mapping genome-wide positions of the noncanonical histone variant H2A.Z enriched at +1 and -1 nucleosomes, we reveal a downstream shift of +1 nucleosomes for the majority of genes in HSV-1 infection. We furthermore confirm that depletion of Pol II alone leads to downstream shifts of +1 nucleosomes in human cells. Thus, changes in chromatin architecture at promoters in HSV-1 infection are likely a consequence of HSV-1-induced depletion of Pol II from the host genome.

Introduction

Herpes simplex virus 1 (HSV-1) is one of nine human herpesviruses, with more than half of the global population being latently infected with HSV-1 (1-4). HSV-1 is known for causing the common cold sores but is also responsible for life-threatening diseases particularly in the immunocompromised (5). The HSV-1 genome consists of 152 kilobases (kb) of double-stranded DNA and encodes for at least 121 large open reading frames (ORFs) and >100 small ORFs (6). Upon lytic infection, the five immediate early (IE) genes ICP0, ICP4, ICP22, ICP27, and ICP47 are expressed and hijack the host gene expression machinery to ensure viral replication during early stages of infection (7-11). This results in recruitment of RNA polymerase II (Pol II) from the host chromatin to viral genomes and a general shutoff of host transcription (7, 9, 11-13). Pol II recruitment to viral genomes is predominantly facilitated by the viral IE protein ICP4 (13), which effectively sequesters Pol II into the viral replication compartment (14). However, ICP4 already depletes Pol II from cellular promoters as early as 2 h post infection (p.i.), i.e. before the onset of viral genome replication, and independent of viral genome copy number (15). The global host transcription shutoff is further exacerbated by ICP22-mediated inhibition of host transcription elongation (16) and the viral *vhs* (virion host shutoff) protein. *vhs* is a nuclease delivered by the tegument of the incoming viral particles and cleaves both viral and host mRNAs (17-19). We recently demonstrated that *vhs* continuously degrades about 30 % of host mRNAs per hour during the first 8 h of high multiplicity lytic infection of primary human fibroblasts (20).

HSV-1 further disturbs host transcription by inducing a widespread disruption of host transcription termination (DoTT) resulting in read-through transcription beyond polyadenylation (pA) sites of host genes for tens of thousands of nucleotides (nt) (21). Read-through transcription can even extend into downstream genes, leading to a seeming

transcriptional induction of these genes. DoTT negatively affects host gene expression in two ways: First, as read-through transcripts are not exported (22), it effectively prevents translation of newly transcribed mRNAs and thus dampens the host transcriptional response to infection. Second, it redirects a large fraction of ongoing Pol II transcription from host gene bodies into downstream intergenic regions and, thus, further exacerbates the depletion of Pol II from host genes. We recently showed that ICP27 is sufficient for inducing DoTT, but DoTT is also observed in absence of ICP27, albeit at substantially reduced levels (23). As cellular stresses also induce transcription downstream of genes (DoG) (22, 24-26), HSV-1-induced read-through transcription in absence of ICP27 presumably results from a virus-induced cellular stress response (27). In contrast to stress-induced DoGs, HSV-1-induced DoTT is associated with a massive increase of chromatin accessibility downstream of genes (denoted as downstream open chromatin regions (dOCRs)) (22). dOCR induction requires strong absolute levels of transcription downstream of genes, thus it is predominantly observed for highly transcribed genes with strong read-through. Treatment with phosphonoacetic acid (PAA) during HSV-1 infection, which inhibits viral DNA replication (28, 29), results in increased dOCR induction (30). As viral DNA redirects Pol II from the host chromatin, PAA treatment mitigates the loss of Pol II from the host genome and thus increases absolute levels of transcription on host genes and – importantly for dOCR induction – read-through regions. Although dOCRs can extend into downstream genes following read-through transcription, this occurs only in cases of very strong read-through transcription into these downstream genes. We recently showed that ICP22 is both required and sufficient for inducing dOCRs in presence of ICP27-induced read-through (30). This discovery was based on extensive ATAC-seq (Assay for Transposase-Accessible Chromatin using sequencing) analysis of both wild-type (WT) HSV-1 infection as well as infection with null mutants for ICP0, ICP22, ICP27, and *vhs*.

As we previously only investigated chromatin accessibility *downstream* of genes, we now further explore these data to investigate changes in chromatin accessibility around host gene promoters. This revealed a broadening of open chromatin regions at the promoter into regions downstream of transcription start sites (TSS) for the majority of host genes. While it was consistently observed in absence of ICP0, ICP22, ICP27, and *vhs*, PAA treatment, which alleviates the HSV-1-induced loss of transcription, substantially reduced the extension of open chromatin at the TSS. Analysis of *de novo* transcription using RNA-seq of chromatin-associated RNA revealed a link of this phenomenon to transcription as (i) more highly expressed genes were more strongly affected and (ii) genes with strong antisense transcription exhibited the opposite effect with a broadening of open chromatin into regions upstream of the TSS. ChIPmentation for the noncanonical histone H2A variant H2A.Z enriched at +1 and -1 nucleosomes (31, 32) indicated that changes in chromatin accessibility reflected a downstream shift of +1 nucleosomes in HSV-1 infection. We observed similar changes in H2A.Z occupancy upon α-amanitin treatment, a deadly toxin found in Amanita mushrooms, which inhibits transcription by preventing translocation of Pol II and triggering degradation of Rpb1, the largest subunit of Pol II (33). Furthermore, Weiner *et al.* previously showed that Pol II depletion in yeast induces downstream shifts of +1 nucleosomes, in particular for highly expressed genes (34). Transcribing Pol II disturbs histone-DNA interactions and at high transcription rates leads to eviction of nucleosomes from the chromatin (35). Weiner *et al.* proposed that Pol II depletion relaxes chromatin allowing nucleosomes to shift to more thermodynamically favorable sites. As nucleosome positioning of highly expressed genes deviates more strongly from *in vitro* nucleosome preferences (36), this explains why these genes showed more pronounced shifts. These results provide strong evidence that depletion of Pol II from host genes during HSV-1 infection leads to the downstream shifts of +1 nucleosomes to more thermodynamically favorable sites.

Results

Widespread extension of chromatin-free regions downstream of transcription start sites

To investigate changes in chromatin accessibility within promoter regions during HSV-1 infection, we re-analyzed our recently published ATAC-seq data (30) for mock and wild-type (WT) HSV-1 infection of human foreskin fibroblasts (HFF) as well as infection with null mutant viruses for the HSV-1 IE proteins ICP0, ICP22, and ICP27 as well as *vhs*. Samples for mock, WT, and ΔICP27 infection were collected at 8 h p.i., while samples for ΔICP0 and ΔICP22 infection were collected at 12 h p.i. as these null-mutant infections progress more slowly. To assess chromatin accessibility changes in promoter regions, we identified genomic regions with differential ATAC-seq read density using our newly published RegCFinder method (37). RegCFinder searches for genomic regions for which the read distribution differs between two conditions (e.g., mock and WT infection) and is targeted towards regions of interest by specifying genomic windows as input (**Sup. Fig. 1a**). For each input window, subregions are identified that show differences in the distribution of reads within this window. Statistical significance for identified subregions is determined by DEXSeq (38). For our purposes, we defined the windows of interest as the ± 3kb promoter region around the TSS of 7,649 human genes. These TSSs were previously defined in our analysis of promoter-proximal Pol II pausing in HSV-1 WT infection (39) based on a re-analysis of published precision nuclear run-on sequencing (PRO-seq) and PROcap-seq (a variation of PRO-seq) data of flavopiridol-treated uninfected HFF. CDK9 inhibition by flavopiridol arrests Pol II in a paused state at the TSS, allowing the mapping of Pol II initiation sites with both PRO-seq and PROcap-seq. Filtering for high-confidence TSSs that were confirmed by both data sets and within a maximum distance of 500 bp to the nearest annotated gene on the same strand identified the major TSS for 7,649 genes. Using these 6 kb promoter windows as input, we applied RegCFinder to our ATAC-seq data for WT and all null-mutant infections in

comparison to mock to identify promoter subregions for each gene that show differences in the distribution of open chromatin between infection and mock. It should be noted that we did not filter these windows beforehand to exclude genes for which dOCRs extended from an upstream gene into their promoter window for two reasons: (i) Since dOCRs represent changes in chromatin accessibility, RegCFinder should also detect them; (ii) The further the distance from the upstream gene, the less pronounced are changes in chromatin accessibility in dOCR regions, making it difficult to distinguish them from background. Any approach we tested to filter promoter windows overlapping with dOCRs from upstream genes before the RegCFinder analysis either excluded too many or too few windows. Thus, we decided to first run RegCFinder and then investigate which of the detected changes were due to induction of dOCRs for upstream genes.

RegCFinder identified 23-24,000 differential subregions (in the following also denoted as RegC, short for regions of change) for each virus infection (WT: 23,357 RegC, ΔICP0: 23,532, ΔICP22: 24,640, ΔICP27: 23,523, Δ*vhs*: 23,716, **Sup. Fig. 1b**). Between 29 and 37 % of these showed a statistically significant difference in read density within the corresponding 6 kb promoter windows in infection compared to mock (multiple testing adjusted p-value (adj. p.) ≤ 0.01, WT: 8,552 RegC, ΔICP0: 6,740, ΔICP22: 5,710, ΔICP27: 7,188, Δ*vhs*: 6,860). These represented between 3,129 (ΔICP22 infection) and 4,391 (WT) genes (**Sup. Fig. 1c**). The lower fraction of statistically significant differential regions in ΔICP22 infection is likely due to the relatively low number of ATAC-seq reads mapped to the host genome compared to the other infections (~3.8-fold fewer, see Supplementary Data 1 in (30)). **Fig. 1a** visualizes the positions of identified RegC for the 4,981 promoter windows containing at least one statistically significant (adj. p. ≤ 0.01) differential region for at least one virus infection compared to mock and **Sup. Fig. 1d** illustrates log2 fold-changes for statistically significant

regions. Here, blue indicates that relative read density in that subregion is increased during virus infection compared to mock (infection>mock, denoted as i-RegC in the following) and red that relative read density in that subregion is higher in mock compared to infection (mock>infection, denoted as m-RegC).

Strikingly, our results showed a highly homogeneous picture for WT and null-mutant infections compared to mock, with changes in the same direction observed at approximately the same locations. To identify distinct patterns of changes in chromatin accessibility, we performed hierarchical clustering on the RegC location heatmap in **Fig. 1a** and selected a cutoff on the dendrogram to obtain 14 clusters identified by visual inspection. To visualize average read density for each cluster, we performed metagene analyses of promoter windows combined with statistics on RegC locations for each cluster (**Fig. 1b,d,f,g, Sup. Fig. 2**). For metagene analyses, each 6 kb input window was divided into 101 bins of ~59 bp. For each bin, ATAC-seq read counts were determined, normalized to sequencing depth, normalized to sum up to 1 for each input window, averaged across all windows in each cluster and then averaged across replicates. For each bin in the promoter window, metagene curves also show which fraction of windows have an i- (blue) or m-RegC (red) at that position in WT infection. Based on the location heatmap and the metagene analyses, we identified three major patterns in changes in chromatin accessibility around promoters during WT infection: (i) ATAC-seq peaks at the TSS that shift and/or broaden into regions downstream of the TSS during HSV-1 infection (clusters 1, 2, 4, 5, 9, 10, 12, 14, a total of 3,472 genes, **Fig. 1b, Sup. Fig. 2a-g,** examples in **Fig. 1c, Sup. Fig. 3a-h**), (ii) ATAC-seq peaks at the TSS that shift and/or broaden into regions upstream of the TSS (clusters 6, 7, 11, a total of 919 genes, **Fig. 1d, Sup. Fig. 2h,i,** examples in **Fig. 1e, Sup. Fig. 3i-k**), and (iii) an increase in chromatin-accessibility both up- and downstream of the TSS peak in infection compared to mock (cluster 13, 126 genes, **Fig. 1f,** example in **Sup. Fig. 3l**). Two clusters (3 and 8, a total of 464 genes) exhibited

a combination of patterns (i) and (ii) with an extension of the TSS peak in both up- and downstream direction (**Fig. 1g, Sup. Fig. 2j, Sup. Fig. 3m,n**).

As a first analysis, we performed motif discovery both for novel and known motifs in m- and i-RegC grouped either by cluster or pattern compared to the background of all promoter windows using HOMER (40), but found no enriched motifs. Functional enrichment analysis for Gene Ontology (GO) terms also yielded no significant results, with the exception of cluster 13 (pattern (iii)). Cluster 13 was enriched for "mRNA splicing via the spliceosome" and related terms, however, this was mainly due to several snRNA genes included in this cluster. Accordingly, when investigating enrichment of clusters for gene types (**Sup. Fig. 1e**), we found that cluster 13 was significantly enriched for snRNA genes (adj. p. = 3×10^{-16}, see Materials and Methods). In contrast, pattern (i) clusters tended to have relatively high fractions of protein-coding genes, with clusters 1, 2, 5, and 9 being statistically significantly enriched. Strikingly, cluster 7 (= most pronounced case of pattern (ii)) was significantly enriched for antisense transcripts (adj. p. = 5×10^{-15}). The two other pattern (ii) clusters 6 and 11 as well as cluster 8 (combined pattern (i) + (ii)) also contained a relatively high fraction of antisense transcripts, although this was not statistically significant. The association of pattern (ii) with antisense transcription is further investigated below.

Most chromatin accessibility changes at promoters are independent of dOCR induction

Next, we evaluated which of the observed changes were due to dOCRs extending into promoter regions. For this purpose, we determined the fraction of promoter windows in each cluster that overlapped with dOCRs of the 1,296 genes for which we previously showed consistent dOCR induction across different HSV-1 strains (30) (**Fig. 2a**). dOCR regions in mock, WT and all null mutant infections (average across two replicates) were identified as previously described (22, 30) (see also Materials and Methods). It is important to note here

that some relatively short dOCRs are also observed in mock infection but these substantially extend during HSV-1 infection. In this analysis, we also included ATAC-seq data obtained in the same experiment for 8 h p.i. WT infection combined with PAA treatment (WT+PAA) to identify dOCR regions that are not as clearly detectable without PAA treatment but may still bias promoter analyses. As ICP22 is required for dOCR induction, overlaps of promoter windows to dOCR regions in ΔICP22 infection were as low as in mock infection. In other virus infections, some clusters showed enrichment for dOCR overlaps that increased with the overall extent of dOCR induction in these viruses. To highlight this trend, WT (± PAA) and null mutant infections are ordered according to the extent of dOCR induction in **Fig. 2a**. No cluster had more than 20% of promoter windows overlapping with dOCRs even with PAA treatment and most had < 5% overlap, indicating that dOCRs represent only a very small fraction of observed changes in chromatin accessibility around promoters.

Interestingly, cluster 13, which exhibited increased chromatin accessibility surrounding the TSS peak (pattern (iii)) also exhibited the strongest enrichment for dOCRs during infection. An example for a gene with dOCRs extending into the promoter is shown in **Sup. Fig. 3l**. Weaker enrichment for dOCRs was also observed for clusters 12 and 14, for which we detected regions with increased chromatin accessibility in infection also upstream of the TSS, in contrast to other pattern (i) clusters (**Sup. Fig. 2f,g,** example with dOCR overlap in **Sup. Fig. 3h**). In contrast, clusters 3 and 8, which showed a broadening of the TSS peak in both up- and downstream direction (combined pattern (i)+(ii), **Fig. 1g**, **Sup. Fig. 2j**) were not associated with dOCR induction. Importantly, in absence of ICP22, which is required for dOCR induction, we generally observed the same trends in chromatin accessibility changes at promoters as for WT and the other null-mutant infections (**Sup. Fig. 4-17**). This largely also applied to clusters 12-14, though a subset of differential regions was no longer observed in ΔICP22 infection. This applied to some (but not all) regions with increased chromatin

accessibility upstream of genes in clusters 12 and 14 and around TSS peaks in cluster 13 (**Fig. 1a, Sup. Fig. 1d, Sup. Fig. 15-17**). Thus, only some chromatin accessibility changes in clusters 12-14 were linked to dOCR induction. As absence of ICP0, ICP27 or *vhs* also had little impact on changes in chromatin accessibility around promoters, we conclude that neither dOCR induction nor activity of ICP0, ICP22, ICP27 or *vhs* alone explain the majority of observed changes in chromatin accessibility at promoters in HSV-1 infection.

Extension of accessible chromatin regions around promoters is linked to transcription

In contrast to the single-gene knockouts, PAA treatment substantially reduced, though not completely abolished, the downstream broadening and/or shift of TSS peaks in pattern (i) clusters and the upstream broadening and/or shift in pattern (ii) clusters (**Fig. 2b,c, Sup. Fig. 4-17**). Furthermore, fold-changes for differential regions were generally less pronounced (**Sup. Fig. 18a**). Exceptions were cluster 13, and parts of cluster 12 and 14, for which chromatin accessibility increased up- (for clusters 12-14) and downstream (for cluster 13) of the TSS peak (**Fig. 2d, Sup. Fig. 15-17**). This is consistent with these clusters being enriched for dOCR induction originating from an upstream gene, which is increased upon PAA treatment. Notably, however, the broadening of the TSS peak into downstream regions in clusters 12 and 14 was greatly reduced by PAA treatment.

Since PAA treatment alleviates the depletion of Pol II from host genomes, we hypothesized that loss of Pol II contributes to the observed changes in chromatin accessibility around promoters in HSV-1 infection. Notably, PAA only reduces expression of late, but not IE and early HSV-1 proteins (28). Thus, activities of IE, early and tegument-delivered proteins can still lead to some loss of host gene transcription in presence of PAA. These activities include depletion of Pol II by ICP4 prior to genome replication (15), loss of Pol II phosphorylation and inhibition of elongation mediated by ICP22 (16), as well as ICP27-induced inhibition of

transcription termination, which redirects Pol II from gene bodies to intergenic regions (21). To correlate transcriptional activity of genes to the observed patterns in chromatin accessibility changes, we analyzed RNA-seq data of chromatin-associated RNA for mock and 8 h p.i. WT HSV-1 infection from our recent study (20). Chromatin-associated RNA depicts ongoing nascent transcription on the chromatin. Furthermore, changes in chromatin-associated RNA better reflect transcriptional changes in HSV-1 infection than total RNA measurements as the latter are confounded by *vhs*-mediated mRNA degradation (20). Our analysis also included the 2,668 genes (denoted as NA group) without significant chromatin accessibility changes that were excluded from **Fig. 1a**. Interestingly, metagene analyses for these genes also revealed a slight broadening of the TSS peak into downstream regions, although this was much less pronounced than for pattern (i) clusters and therefore not detected by RegCFinder (**Sup. Fig. 18b**). We analyzed gene expression values in mock and WT infection (quantified as FPKM = fragments per kilobase million mapped reads, **Fig. 2e**) as well as log2 fold-changes in gene expression between WT and mock infection (**Sup. Fig. 18c**). Furthermore, we hypothesized that pattern (ii) was shaped by antisense transcription since pattern (ii) essentially represented the mirror image of pattern (i) (mirrored at a vertical axis through the TSS), cluster 7 (most pronounced pattern (ii)) was enriched for antisense transcripts (**Sup. Fig. 1e**), and several pattern (ii) examples showed overlapping or nearby genes on the opposite strand (e.g. **Fig. 1e**). We thus also calculated the ratio of sense to antisense transcription in promoter windows for all genes. For this purpose, promoter windows were divided into the regions down- and upstream of the TSS and expression was determined in sense direction for the downstream region (=DSR) and in antisense direction for the upstream region (=UAR). Log2 ratios of DSR to UAR expression are shown in **Fig. 2f**.

We observed no consistent differences in log2 gene expression fold-changes associated with any of the patterns in chromatin accessibility changes (**Sup. Fig. 18c**). While cluster 1 (pattern (i)) showed a significant decrease in log2 fold-changes compared to other genes, the remaining pattern (i) clusters showed either no significant difference or a significant increase in log2 fold-changes (cluster 9). Similarly, although one pattern (ii) cluster showed a significant decrease in log2 fold-changes (cluster 6), the other two clusters did not. It should be noted here that log2 fold-changes represent relative changes in gene expression compared to all other genes. Thus, genes with positive log2 fold-changes are either increased in expression or less decreased compared to all other genes, while genes with negative log2 fold-changes are more decreased in expression compared to all other genes. In contrast, gene expression levels differed significantly between patterns in both mock and WT infection. Most pattern (i) clusters as well as cluster 3 (combined pattern (i)+(ii)) exhibited median expression levels above average in mock (**Fig. 2e**), which was statistically significant for 5 clusters. In contrast, clusters 6, 7 (pattern (ii)) and 8 (combined pattern (i)+(ii)) exhibited relatively low expression values, with cluster 7 genes having significantly lower expression. Genes without significant chromatin accessibility changes (NA group) also showed significantly lower expression, albeit not as low as cluster 7. These differences between clusters/patterns were generally maintained in HSV-1 infection at lower overall expression levels, consistent with the absence of differences in gene expression fold-changes between most clusters.

Strikingly, when investigating DSR to UAR ratios (**Fig. 2f**), we found that all pattern (ii) clusters had significantly lower DSR to UAR ratios than remaining genes, in particular than those with pattern (i). In part this was due to their lower expression as the ratio to background transcription on the antisense strand is lower. Lower expression in WT infection also explains why log2 DSR:UAR ratios were closer to zero in WT infection for all clusters. However, for

cluster 7, which represented the most pronounced pattern (ii) cluster, the log2 DSR:UAR ratios were commonly negative, i.e. antisense transcription upstream of the TSS was higher than sense transcription downstream of the TSS. This suggests that pattern (ii) effectively represents pattern (i) for the genes on the antisense strand. Notably, for clusters 3 and 8, which we classified as showing both pattern (i) and (ii) (or pattern (i) in both sense and antisense direction), DSR:UAR ratios were generally lower than for pattern (i) clusters, albeit still higher than for pattern (ii) clusters and genes without significant chromatin changes (NA group). For these genes the extension of accessible chromatin at the promoter was also more pronounced in sense than in antisense direction. In summary, these results indicate that HSV-1 infection leads to an extension of the accessible chromatin around promoters for the majority of genes in the dominant direction of transcription. Here, highly expressed genes appear to be most strongly affected.

To investigate how early in infection changes in chromatin accessibility around promoters can be detected, we ran RegCFinder on an ATAC-seq time-course for 1, 2, 4, 6, and 8 h p.i. WT infection from our previous publication (22) (**Fig. 3a,b**). While barely any significant differential regions were identified at 1 and 2 h p.i., 1,963 significant regions were identified in 1,249 promoter windows by 4 h p.i. and 7,558 significant regions in 3,989 promoter windows by 8 h p.i. (**Fig. 3b**). Log2 fold-changes for significant differential regions generally reflected the patterns observed in the analysis for WT and null mutant infections (**Fig. 3a**). The same applied when we separately determined fold-changes and significance on the time-course ATAC-seq data for the differential regions determined for WT vs. mock from our initial analysis (**Sup. Fig. 19**) and when we performed metagene analyses for the clusters from **Fig. 1a (Sup. Fig. 20**, example genes in **Sup. Fig. 21)**. Although the changes in chromatin accessibility at 8 h p.i. of the time-course were less pronounced than for the original WT vs. mock comparison at 8 h p.i., this nevertheless confirms the changes in

chromatin accessibility around promoters in HSV-1 infection in an independent experiment. Furthermore, it reveals that these changes begin to manifest between 2 and 4 h p.i. We previously showed that transcriptional activity on host genes drops substantially in the first 4 h of infection to only 40% of transcription in uninfected cells, which was further halved until 8 h p.i. (20). Thus, the onset of the extension of accessible chromatin regions at promoters into downstream (for pattern (i)) and upstream (for pattern (ii) regions coincides with the onset of the drop in host transcription during infection.

HSV-1 infection induces a downstream shift of +1 nucleosomes

The HSV-1-induced changes in chromatin accessibility at promoters suggest a broadening of the nucleosome-free region around promoters in either sense (pattern (i)) or antisense (pattern (ii)) direction. Consistent with this, we observed downstream and upstream shifts for pattern (i) and (ii) clusters, respectively, in the nucleosome-depleted regions at promoters in H3K36me3 ChIPmentation data for mock and 8 h WT HSV-1 infection from our previous study (30) (**Sup. Fig. 22**). H3K36me3 marks H3 histones on actively transcribed genes (41). These changes in nucleosome-free regions require a shift in nucleosome positioning, in particular for +1 or -1 nucleosomes. Several studies performed in yeast previously investigated the role of transcriptional activity on nucleosome positioning (42-44). In particular, Weiner *et al*. reported a downstream shift of +1 nucleosomes upon Pol II depletion in yeast (34). Here, the strongest downstream shifts were observed for very highly expressed genes, consistent with our observation that pattern (i) was associated with higher gene expression (**Fig. 2e**). To investigate whether changes in chromatin accessibility at promoters during HSV-1 infection were linked to shifts in +1 and -1 nucleosome positions, we performed ChIPmentation in HFF for mock and 8 h p.i. WT infection with an antibody recognizing the C-terminal part of the non-canonical histone H2A.Z (n=3 replicates). H2A.Z is highly enriched at gene promoters at -1 and +1 nucleosome positions (31, 32) and is

encoded by two genes, whose protein products H2A.Z.1 and H2A.Z.2 differ by only three amino acids. While their genomic occupancy patterns are similar, there are quantitative differences with H2A.Z.1 being more abundant at active promoters than H2A.Z.2 (45). Since the C-terminal regions of H2A.Z.1 and H2A.Z.2 differ only by the last amino acid, the antibody used for ChIPmentation recognizes both isoforms. A metagene analysis of all analyzed promoter windows showed the expected distribution of H2A.Z occupancy in mock infection with two peaks on both sides of the TSS, corresponding to -1 and +1 nucleosome positions (**Sup. Fig. 23a**).

Application of RegCFinder to H2A.Z ChIPmentation data generally identified a relative increase in H2A.Z downstream of the TSS during infection and a relative decrease upstream of the TSS for pattern (i) and combined pattern (i)+(ii) clusters (**Fig. 4a**, log2 fold-changes for differential regions shown in **Sup. Fig. 23b**, examples in **Fig 4b**, **Sup. Fig. 24a-g,k,l**). Metagene analyses showed that this reflected a downstream shift and broadening of +1 nucleosome peaks as well as a relative increase of +1 nucleosome peaks compared to -1 nucleosome peaks (**Fig. 4d**, **Sup. Fig. 23c-i,m,n**). In contrast, cluster 7 (most pronounced pattern (ii) cluster) showed the opposite trend with relative increases in H2A.Z upstream of the TSS and decreases downstream of the TSS (example in **Fig 4c**). Consistent with pattern (ii) representing pattern (i) in antisense direction, the metagene analysis showed an upstream shift and broadening of the -1 nucleosome peak and a relative increase of the -1 nucleosome peak compared to the +1 nucleosome peak (**Fig. 4e**). However, this was only observed for few genes in cluster 6 and cluster 11 (**Fig. 4a**, **Sup. Fig. 23j,k**, examples in **Fig. 4c, Sup. Fig. 24h,i**), which fits with the observation that pattern (ii) in the ATAC-seq data was also much less pronounced for these clusters. In contrast to pattern (i) and (ii), pattern (iii) in the ATAC-seq data (cluster 13) was not associated with notable changes in H2A.Z (**Sup. Fig. 23l**, example in **Sup. Fig. 24j**), indicating that it is not shaped by shifts in +1 and/or -1

nucleosome positioning. This is consistent with pattern (iii) being at least partly associated with dOCR induction for upstream genes, which we previously linked to impaired nucleosome repositioning following Pol II transcription downstream of genes (30).

In summary, our data suggest that the alterations in chromatin accessibility around promoters result from an extension of the nucleosome-free region around promoters due to downstream and upstream shifts of either +1 or -1 nucleosomes. Here, the direction of shift depends on whether sense or antisense transcription represents the dominant direction of transcription at this genome position. Notably, a recent study in yeast proposed that -1 nucleosomes should actually be considered +1 nucleosomes for antisense transcription (46). We hypothesized that – similar to what was previously observed for yeast – the loss of Pol II from host promoters during HSV-1 infection induced the shift of +1 and -1 nucleosome positions. To confirm that inhibition of transcription alone can lead to similar shifts of +1 and -1 nucleosomes in human cells, we re-analyzed published H2A.Z ChIP-seq data of HCT116 cells with and without α-amanitin treatment from the study by Lashgari *et al.* (47). They previously showed that α-amanitin treatment leads to reduced Pol II levels at gene TSSs and increased incorporation of H2A.Z at TSSs of transcribed genes. However, they only analyzed changes in absolute H2A.Z levels at TSS promoters and did not focus on changes in +1 and -1 nucleosome positioning. Metagene and RegCFinder analyses of the H2A.Z ChIP-seq data for our clusters indeed showed a similar trend upon α-amanitin treatment as during HSV-1 infection (**Fig. 4f,g, Sup. Fig. 25,** examples are shown in **Sup. Fig. 26**). Pattern (i) and pattern (i)+(ii) clusters showed a massive broadening of the +1 nucleosome peak into downstream regions, even more pronounced than what is observed upon HSV-1 infection. In addition, they also showed a less pronounced broadening of -1 nucleosome peaks. Similarly, pattern (ii) clusters showed a strong broadening of both -1 and +1 nucleosome peaks into upstream regions. In case of cluster 7 (strongest pattern (ii)), the broadening was much more pronounced for the -1

nucleosome (i.e. the +1 nucleosome in antisense direction) than for the +1 nucleosome (i.e. the -1 nucleosome in antisense direction). This analysis confirms that depletion of Pol II from promoters leads to a downstream shift of +1 nucleosomes in human cells. Together with the mitigating effect of PAA treatment on the chromatin accessibility changes in HSV-1 infection and the timing of onset, our results thus provide strong evidence that the shift of +1 and -1 nucleosomes in the direction of transcription in HSV-1 infection is a consequence of Poll II depletion from host chromatin.

Discussion

Previously, we showed that HSV-1 infection disrupts chromatin architecture downstream of genes with strong read-through transcription. In this study, we reveal that chromatin architecture is also substantially altered at host gene promoters during HSV-1 infection. Here, 57% of genes showed a statistically significant change in the distribution of chromatin accessibility at promoters in WT HSV-1 infection and metagene analyses indicated similar but less pronounced changes even for genes without statistically significant changes. In essence, we identified three types of changes: Most genes showed a shift of the TSS peak and/or broadening of chromatin accessibility into regions downstream of the TSS (pattern (i)), while ~900 genes showed the opposite trend with a shift of the TSS peak and/or broadening of chromatin accessibility into regions upstream of the TSS (pattern (ii)). A further ~460 genes exhibited a combination of pattern (i) and (ii), with the broadening of accessible chromatin in downstream direction being more pronounced than in upstream direction. Only a small set of genes (126 genes) showed relative increases in chromatin accessibility up- and downstream of the TSS, which could partly be attributed to overlaps with dOCRs from upstream genes and partly to an enrichment for (short) non-coding RNAs for which promoter windows were larger than the actual gene length. We thus did not further investigate this pattern.

As patterns (i) and (ii) were still observed in absence of ICP22, which is necessary for dOCR induction, these are not artefacts of dOCRs extending into downstream genes. On the contrary, PAA treatment, which increases dOCR induction, substantially reduced – though not completely abolished – pattern (i) and (ii). In contrast, knockdown of neither ICP0, ICP22, ICP27 nor *vhs* substantially affected pattern (i) and (ii). This led us to hypothesize that the loss of Pol II from host genes during HSV-1 infection, which is alleviated by PAA, causes the widespread extension of open chromatin at host gene promoters. Analysis of transcriptional activity using RNA-seq of chromatin-associated RNA revealed that pattern (i) and (ii) are indeed linked to transcription, with pattern (i) associated with more highly expressed genes and pattern (ii) associated with genes with strong antisense transcription on the opposite strand. In case of cluster 7, for which pattern (ii) was most pronounced, antisense transcription was indeed much higher than sense transcription. This was not due to the widespread induction of antisense transcription we previously reported in HSV-1 infection (48), but these genes already exhibited strong transcription in antisense direction in uninfected cells originating from overlapping genes on opposite strands or bidirectional promoters. Thus, pattern (ii) is essentially just pattern (i) for the genes on the antisense strand.

Since the broadening of chromatin accessibility in promoter regions suggested an extension of nucleosome-free regions at promoters, we mapped +1 and -1 nucleosome positions by ChIPmentation of the H2A.Z histone variant enriched at these nucleosomes. Analysis of H2A.Z occupancy indeed showed a downstream shift of +1 nucleosomes for pattern (i) genes in HSV-1 infection and an upstream shift of -1 nucleosomes for genes with most pronounced pattern (ii) (cluster 7). This further confirmed that pattern (ii) just represents pattern (i) for genes on the antisense strand. It is also consistent with recent results from yeast by Bagchi *et al.* that -1 H2A.Z-containing nucleosomes should actually be considered as +1 nucleosomes

for antisense transcription (46). Downstream shifts of +1 nucleosomes have previously been reported upon Pol II degradation in yeast by Weiner *et al.* (34), in particular for highly expressed genes. Re-analysis of published H2A.Z ChIP-seq data with and without α-amanitin-induced depletion of Pol II from gene promoters confirmed that loss of Pol II alone is sufficient to induce downstream shifts of +1 nucleosomes in human cells. Moreover, for genes with dominant antisense transcription (cluster 7), it resulted in upstream shifts of -1 nucleosomes. Here, the broadening of H2A.Z peaks in both HSV-1 infection and upon α-amanitin treatment, respectively, indicate a less precise positioning of corresponding nucleosomes. This was more pronounced upon α-amanitin treatment and also observed for -1 nucleosomes, suggesting that loss of Pol II upon α-amanitin treatment is more complete than in HSV-1 infection.

The +1 nucleosome has been shown to play a role in promoter-proximal Pol II pausing, which occurs between the promoter and the +1 nucleosome (49). It is thus tempting to speculate that the downstream shifts in +1 nucleosomes we observed in this study may provide an explanation for the downstream shift in Pol II pausing in HSV-1 infection we recently reported (39). Notably, there are a few parallels between the downstream shifts of +1 nucleosomes and changes in Pol II pausing during HSV-1 infection. Both appear to be established relatively early in infection, with the extension of the nucleosome-free region detectable at 4 h p.i. but not at 2 h p.i. in our ATAC-seq data and the downstream shift of Pol II pausing clearly detectable in PRO-seq data at 3 h p.i. but not yet at 1.5 h p.i. (49). Furthermore, both +1 nucleosomes and Pol II pausing sites, which are well-positioned in uninfected cells, appear much less well-positioned in HSV-1 infection. In this way, both phenomena would largely be a bystander effect of the loss of host transcriptional activity and not necessarily play a functional role for HSV-1 infection. Alternatively, the shifts in +1 nucleosomes might also be linked to the mobilization of H1, H2 (including H2A.Z) and H4

histones during HSV-1 infection (50-52), which has been proposed to serve as a source of histones for viral chromatin assembly. In any case, our study highlights that HSV-1 infection impacts chromatin architecture at promoters independently of the widespread changes downstream of genes mediated by ICP22.

Materials and Methods

Previously published sequencing data analyzed in this study

ATAC-seq for mock and WT HSV-1 infection (strain 17, 8 h p.i.), WT infection with 8 h PAA treatment, infection with ICP0-null mutant (ΔICP0, strain 17, (53), 12 h p.i.), ICP22-null mutant (ΔICP22, R325, strain F, (54), 12 h p.i.), ICP27-null mutant (ΔICP27, strain KOS, (55), 8 h p.i.) and *vhs*-null mutant (Δvhs, strain 17, (56)) in of HFF were taken from our recent publication (30) (n=2 apart from ΔICP22 infection with n=4, GEO accession: GSE185234). ATAC-seq data for mock and WT HSV-1 infection of HFF at 1, 2, 4, 6 and 8 h p.i. WT infection (n=2 replicates, GEO accession: GSE100611) and chromatin-associated RNA-seq data for mock and 8 h p.i. WT infection (GEO accession: GSE100576) were taken from our previous publication (22). H3K36me3 ChIPmentation data for mock and 8 h p.i. WT infection of HFF were also taken from our recent publication (30) (n=3, GEO accession: GSE185246). H2A.Z ChIP-seq data of untreated and α-amanitin-treated HCT116 cells were taken from the study by Lashgari *et al.* (47) (n=2, GSE101427).

ChIPmentation, library preparation and sequencing

Two days prior to infection, two million HFF cells were seeded in 15 cm dishes. At the day of infection, cells had expanded to ~80% confluency. Cells were infected with the respective viruses as described in results section (n=3). At 8 p.i., cells were fixed for 10 minutes at room temperature by adding 1% formaldehyde (final) directly to the medium. Cells were scraped in 1mL of ice-cold 1x PBS containing protease inhibitor cocktail (1x) (Roche #11836153001)

with an additional 1mM phenylmethylsulfonyl fluoride (PMSF). Cells were pelleted at 1500 rpm for 20 min at 4 °C. Supernatant was aspirated and cell pellets were frozen in liquid N_2. Cell pellets were resuspended in 1.5 mL 0.25% [w/v] SDS sonication buffer (10 mM Tris pH=8.0, 0.25% [w/v] SDS, 2 mM EDTA) with 1x protease inhibitors and 1 mM additional PMSF and incubated on ice for 10 minutes. Cells were sonicated in fifteen 1 minute intervals, 25% amplitude, with Branson Ultrasonics SonifierTM S-450 until most fragments were in the range of 200-700 bp as determined by agarose gel electrophoresis. Two million cells used for the preparation of the ChIPmentation libraries were diluted 1:1.5 with equilibration buffer (10 mM Tris, 233 mM NaCl, 1.66% [v/v] Triton X-100, 0.166% [w/v] sodium deoxycholate, 1 mM EDTA, protease inhibitors) and spun at 14,000x g for 10 minutes at 4 °C to pellet insoluble material. Supernatant was transferred to a new 1.5 mL screw-cap tube and topped up with RIPA-LS (10 mM Tris-HCl pH 8.0, 140 mM NaCl, 1 mM EDTA pH 8.0, 0.1% [w/v] SDS, 0.1% [w/v] sodium deoxycholate, 1% [v/v] Triton X-100, protease inhibitors) to 200 µL. Input and gel samples were preserved. Lysates were incubated with 1µg/IP of anti-H2A.Z antibody (Diagenode, #C15410201) on a rotator overnight at 4 °C.

Dependent on the added amount of antibody, the amount of Protein A magnetic beads (ThermoFisher Scientific #10001D) was adjusted (e.g. for 1-2 µg of antibody/IP = 15 µL of beads) and blocked overnight with 0.1% [w/v] bovine serum albumin in RIPA buffer. On the following day, beads were added to the IP samples for 2 h on a rotator at 4 °C to capture the antibody-bound fragments. The immunoprecipitated chromatin was subsequently washed twice with 150 µL each of ice-cold buffers RIPA-LS, RIPA-HS (10 mM Tris-HCl pH 8.0, 50 0mM NaCl, 1 mM EDTA pH 8.0, 0.1% [w/v] SDS, 0.1% [v/v] sodium deoxycholate, 1% [v/v] Triton X-100), RIPA-LiCl (10 mM Tris-HCl pH 8.0, 250 mM LiCl, 1 mM EDTA pH 8.0, 0.5% [w/v] sodium deoxycholate, 0.5% [v/v] Nonidet P-40) and 10 mM Tris pH 8.0

containing protease inhibitors. Beads were washed once more with ice-cold 10 mM Tris pH 8.0 lacking inhibitors and transferred into new tubes.

Beads were resuspended in 25 μL of the tagmentation reaction mix (Nextera DNA Sample Prep Kit, Illumina) containing 5 μL of 5x Tagmentation buffer, 1 μL of Tagment DNA enzyme, topped up with H_2O to the final volume and incubated at 37 °C for 10 minutes in a thermocycler. Beads were mixed after 5 minutes by gentle pipetting. To inactivate the Tn5 enzyme, 150 μL of ice-cold RIPA-LS was added to the tagmentation reaction. Beads were washed twice with 150 μL of RIPA-LS and 1x Tris-EDTA and subjected to de-crosslinking by adding 100 μL ChIPmentation elution buffer (160 mM NaCl, 40 μg/mL RNase A (Sigma-Aldrich #R4642), 1x Tris-EDTA (Sigma #T9285) and incubating for 1h at 37 °C followed by overnight shaking at 65 °C. The next day, 4 mM EDTA and 200 μg/mL Proteinase K (Roche, #03115828001) were added, and samples incubated for another 2h at 45 °C with 1000 rpm shaking. Supernatant was transferred into a new tube and another 100 μL of ChIPmentation elution buffer was added for another hour at 45 °C with 1000 rpm shaking. DNA was isolated with MinElute PCR Purification Kit (Qiagen #28004) and eluted in 21 μL of H_2O.

DNA for the final library was prepared with 25 μL NEBNext Ultra II Q5 Master Mix, 3.75 μL IDT custom primer i5_n_x (10 μM); 3.75 μL IDT custom primer i7_n_x (10 μM); 3.75 μL H_2O and 13.75 μL ChIPmentation DNA. The Cq value obtained from the library quantification, rounded up to the nearest integer plus one additional cycle, was used to amplify the rest of the ChIPmentation DNA. Library qualities were verified by High Sensitivity DNA Analysis on the Bioanalyzer 2100 (Agilent) before performing sequencing on NextSeq 500 (paired-end 35bp reads) at the Core Unit Systemmedizin, Würzburg, Germany. All samples were sequenced at equimolar ratios.

Read alignment

The read alignment pipeline was implemented and run in the workflow management system Watchdog (57, 58) as already previously described (39). Public sequencing data were downloaded from SRA using the sratoolkit version 2.10.8. Sequencing reads were aligned against the human genome (GRCh37/hg19), the HSV-1 genome (Human herpesvirus 1 strain 17, GenBank accession code: JN555585) and human rRNA sequences using ContextMap2 version 2.7.9 (59) (using BWA as short read aligner (60) and allowing a maximum indel size of 3 and at most 5 mismatches). For the two repeat regions in the HSV-1 genome, only one copy was retained each, excluding nucleotides 1–9,213 and 145,590–152,222 from the alignment. SAM output files of ContextMap2 were converted to BAM files using samtools (61). Read coverage in bedGraph format was calculated from BAM files using BEDTools (62). Subregions of promoter windows (TSS ± 3 kb) with differential read coverage in ATAC-seq and H2A.Z ChIPmentation/-seq data were determined with RegCFinder (37). For this purpose, RegCFinder was applied to ATAC-seq data for all pairwise comparisons of mock to WT and null mutant infections as well as mock to each timepoint of infection for the time-course data and to H2A.Z ChIPmentation and ChIP-seq data for the comparison of mock and WT infection as well as untreated and α-amanitin-treated HCT116 cells.

Data plotting and statistical analysis

All figures were created in R and all statistical analyses were performed in R (63). Read coverage plots were created using the R Bioconductor package Gviz (64).

Metagene and clustering analysis

Metagene analyses were performed as previously described (65) using the R program developed for this previous publication (available with the Watchdog *binGenome* module in the Watchdog module repository (https://github.com/watchdog-wms/watchdog-wms-

modules/). For promoter region analyses, the regions −3 kb to +3 kb of the TSS were divided into 101 equal-sized bins for each gene. For each bin, the average coverage per genome position was calculated and bin read coverages were then normalized by dividing by the total sum of all bins. Metagene curves for each replicate were created by averaging results for corresponding bins across all genes in a cluster/group and then averaged across replicates. For hierarchical clustering analysis, RegCFinder profiles of differential regions were calculated for each promoter window and comparison by setting each position in an m-RegC to 1, in an i-RegC to -1 and all other positions to 0. RegCFinder profiles of each promoter window for each comparison were concatenated into one row in the matrix. Hierarchical clustering of the resulting matrix was then performed using the hclust function in R according to Euclidean distances and Ward's clustering criterion.

Motif discovery and enrichment analysis

Motif discovery was performed for each cluster separately for the i- and m-RegC regions using findMotifsGenome.pl script of the Homer suite (40), with our 7,649 input promoter windows as background. For this purpose, we used the hg19 annotation provided by Homer and automated trimming of input windows was disabled. Significant motifs were identified at a q-value (=False Discovery Rate (FDR) calculated with the Benjamini-Hochberg method (66)) cutoff of 0.01. Over-representation of Gene Ontology (GO) terms was performed separately for each cluster using the g:Profiler webserver (67) and the R package gprofiler2 (68), which provides an R interface to the webserver. As background gene list, the genes corresponding to our 7,649 input promoter windows were provided. P-values were corrected for multiple testing using the Benjamini-Hochberg method (66) and significantly over-represented GO terms were identified at an multiple testing adjusted p-value cutoff of 0.001. Enrichment of gene types (obtained from the Ensembl annotation (version 87 for GRCh37))

within clusters was determined using one-sided Fisher's exact tests (with alternative = greater). P-values were again corrected for multiple testing using the Benjamini-Hochberg method and an adjusted p-value cutoff of 0.001 was used.

Analysis of downstream open chromatin regions (dOCRs)

Open chromatin regions (OCRs) were determined from ATAC-seq data by first converting BAM files with mapped reads to BED format using BEDTools (69) and then determining enriched regions from these BED files using F-Seq with default parameters (70). dOCRs for individual genes were calculated from OCRs as previously described (22, 30). In brief, dOCRs are determined for genes by first assigning all OCRs overlapping with the 10 kb downstream of a gene to this gene. Second, OCRs starting at most 5 kb downstream of the so far most downstream OCR of a gene are also assigned to this gene. In both steps, individual OCRs can be assigned to multiple genes. The second step is iterated until no more OCRs can be assigned. The dOCR of a gene is then defined as the region from the gene 3'end to the end of the most downstream OCR assigned to this gene.

Gene expression analysis

Number of fragments (=read pairs) per gene were determined from mapped paired-end RNA-seq reads in a strand-specific manner using featureCounts (71) and gene annotations from Ensembl (version 87 for GRCh37). For genes, all fragments overlapping exonic regions on the corresponding strand by ≥ 25bp were counted for the corresponding gene. Fold-changes in gene expression and statistical significance of changes were determined using DESeq2 (72) and p-values were adjusted for multiple testing using the method by Benjamini and Hochberg (66). Gene expression was quantified in terms of fragments per kilobase of exons per million

mapped reads (FPKM). Only reads mapped to the human genome were counted for the total number of mapped reads for FPKM calculation.

Acknowledgements

This work was funded by the Deutsche Forschungsgemeinschaft (DFG, German Research Foundation) in the framework of the Research Unit FOR5200 DEEP-DV (443644894) projects FR 2938/11-1 to C.C.F. and DO 1275/12-1 to L.D.

Competing interests

The authors declare no competing interests.

References

1. Roizman B KD, RJ W. Herpes Simplex Viruses. In: Knipe DM HP, editor. Fields Virology. 5th. Philadelphia: Lippincott Williams & Wilkins; 2007. p. 2501-601.

2. Pellet PE RB. Herpesviridae. In: Knipe DM HP, editor. Fields Virology. 6th. Philadelphia: Wolters Kluwer Health/Lippincott Williams & Wilkins; 2013. p. 1802-2128.

3. Ablashi D, Agut H, Alvarez-Lafuente R, Clark DA, Dewhurst S, DiLuca D, et al. Classification of HHV-6A and HHV-6B as distinct viruses. Arch Virol. 2014;159(5):863-70.

4. Korr G, Thamm M, Czogiel I, Poethko-Mueller C, Bremer V, Jansen K. Decreasing seroprevalence of herpes simplex virus type 1 and type 2 in Germany leaves many people susceptible to genital infection: time to raise awareness and enhance control. BMC Infect Dis. 2017;17(1):471.

5. Whitley RJ, Roizman B. Herpes simplex virus infections. Lancet. 2001;357(9267):1513-8.

6. Whisnant AW, Jürges CS, Hennig T, Wyler E, Prusty B, Rutkowski AJ, et al. Integrative functional genomics decodes herpes simplex virus 1. Nat Commun. 2020;11(1):2038.

7. Spencer CA, Dahmus ME, Rice SA. Repression of host RNA polymerase II transcription by herpes simplex virus type 1. J Virol. 1997;71(3):2031-40.

8. Rice SA, Davido DJ. HSV-1 ICP22: hijacking host nuclear functions to enhance viral infection. Future Microbiol. 2013;8(3):311-21.

9. Abrisch RG, Eidem TM, Yakovchuk P, Kugel JF, Goodrich JA. Infection by Herpes Simplex Virus 1 Causes Near-Complete Loss of RNA Polymerase II Occupancy on the Host Cell Genome. J Virol. 2015;90(5):2503-13.

10. Dembowski JA, DeLuca NA. Selective recruitment of nuclear factors to productively replicating herpes simplex virus genomes. PLoS Pathog. 2015;11(5):e1004939.

11. Birkenheuer CH, Danko CG, Baines JD. Herpes Simplex Virus 1 Dramatically Alters Loading and Positioning of RNA Polymerase II on Host Genes Early in Infection. J Virol. 2018;92(8).

12. Rivas HG, Schmaling SK, Gaglia MM. Shutoff of Host Gene Expression in Influenza A Virus and Herpesviruses: Similar Mechanisms and Common Themes. Viruses. 2016;8(4):102.

13. Dremel SE, DeLuca NA. Herpes simplex viral nucleoprotein creates a competitive transcriptional environment facilitating robust viral transcription and host shut off. Elife. 2019;8.

14. McSwiggen DT, Hansen AS, Teves SS, Marie-Nelly H, Hao Y, Heckert AB, et al. Evidence for DNA-mediated nuclear compartmentalization distinct from phase separation. eLife. 2019;8:e47098.

15. Dremel SE, DeLuca NA. Herpes simplex viral nucleoprotein creates a competitive transcriptional environment facilitating robust viral transcription and host shut off. eLife. 2019;8:e51109.

16. Isa NF, Bensaude O, Aziz NC, Murphy S. HSV-1 ICP22 Is a Selective Viral Repressor of Cellular RNA Polymerase II-Mediated Transcription Elongation. Vaccines. 2021;9(10):1054.

17. Kwong AD, Frenkel N. Herpes simplex virus-infected cells contain a function(s) that destabilizes both host and viral mRNAs. Proc Natl Acad Sci U S A. 1987;84(7):1926-30.

18. Oroskar AA, Read GS. Control of mRNA stability by the virion host shutoff function of herpes simplex virus. J Virol. 1989;63(5):1897-906.

19. Feng P, Everly DN, Jr., Read GS. mRNA decay during herpesvirus infections: interaction between a putative viral nuclease and a cellular translation factor. J Virol. 2001;75(21):10272-80.

20. Friedel CC, Whisnant AW, Djakovic L, Rutkowski AJ, Friedl MS, Kluge M, et al. Dissecting Herpes Simplex Virus 1-Induced Host Shutoff at the RNA Level. J Virol. 2021;95(3).

21. Rutkowski AJ, Erhard F, L'Hernault A, Bonfert T, Schilhabel M, Crump C, et al. Widespread disruption of host transcription termination in HSV-1 infection. Nat Commun. 2015;6:7126.

22. Hennig T, Michalski M, Rutkowski AJ, Djakovic L, Whisnant AW, Friedl MS, et al. HSV-1-induced disruption of transcription termination resembles a cellular stress response but selectively increases chromatin accessibility downstream of genes. PLoS Pathog. 2018;14(3):e1006954.

23. Wang X, Hennig T, Whisnant AW, Erhard F, Prusty BK, Friedel CC, et al. Herpes simplex virus blocks host transcription termination via the bimodal activities of ICP27. Nat Commun. 2020;11(1):293.

24. Vilborg A, Passarelli MC, Yario TA, Tycowski KT, Steitz JA. Widespread Inducible Transcription Downstream of Human Genes. Mol Cell. 2015;59(3):449-61.

25. Rosa-Mercado NA, Zimmer JT, Apostolidi M, Rinehart J, Simon MD, Steitz JA. Hyperosmotic stress alters the RNA polymerase II interactome and induces readthrough transcription despite widespread transcriptional repression. Mol Cell. 2021;81(3):502-13 e4.

26. Hadar S, Meller A, Saida N, Shalgi R. Stress-induced transcriptional readthrough into neighboring genes is linked to intron retention. iScience. 2022;25(12):105543.

27. Wu N, Watkins SC, Schaffer PA, DeLuca NA. Prolonged gene expression and cell survival after infection by a herpes simplex virus mutant defective in the immediate-early genes encoding ICP4, ICP27, and ICP22. Journal of Virology. 1996;70(9):6358-69.

28. Honess RW, Watson DH. Herpes simplex virus resistance and sensitivity to phosphonoacetic acid. Journal of Virology. 1977;21(2):584-600.

29. Becker Y, Asher Y, Cohen Y, Weinberg-Zahlering E, Shlomai J. Phosphonoacetic Acid-Resistant Mutants of Herpes Simplex Virus: Effect of Phosphonoacetic Acid on Virus Replication and In Vitro Deoxyribonucleic Acid Synthesis in Isolated Nuclei. Antimicrobial Agents and Chemotherapy. 1977;11(5):919-22.

30. Djakovic L, Hennig T, Reinisch K, Milic A, Whisnant AW, Wolf K, et al. The HSV-1 ICP22 protein selectively impairs histone repositioning upon Pol II transcription downstream of genes. Nat Commun. 2023;14(1):4591.

31. Barski A, Cuddapah S, Cui K, Roh TY, Schones DE, Wang Z, et al. High-resolution profiling of histone methylations in the human genome. Cell. 2007;129(4):823-37.

32. Raisner RM, Hartley PD, Meneghini MD, Bao MZ, Liu CL, Schreiber SL, et al. Histone variant H2A.Z marks the 5' ends of both active and inactive genes in euchromatin. Cell. 2005;123(2):233-48.

33. Bensaude O. Inhibiting eukaryotic transcription. Which compound to choose? How to evaluate its activity? Transcription. 2011;2(3):103-8.

34. Weiner A, Hughes A, Yassour M, Rando OJ, Friedman N. High-resolution nucleosome mapping reveals transcription-dependent promoter packaging. Genome Res. 2010;20(1):90-100.

35. Schwabish MA SK. Evidence for eviction and rapid deposition of histones upon transcriptional elongation by RNA polymerase II. Mol Cell Biol. 2004;24(23):10111-7.

36. Kaplan N MI, Fondufe-Mittendorf Y, Gossett AJ, Tillo D, Field Y, LeProust EM, Hughes TR, Lieb JD, Widom J, Segal E. The DNA-encoded nucleosome organization of a eukaryotic genome. Nature. 2008;458(7236):362-6.

37. Weiss E, Friedel CC. RegCFinder: targeted discovery of genomic subregions with differential read density. Bioinform Adv. 2023;3(1):vbad085.

38. Anders S RA, Huber W. Detecting differential usage of exons from RNA-seq data. Genome Research. 2012;22(10):2008-17.

39. Weiss E, Hennig T, Grassl P, Djakovic L, Whisnant AW, Jurges CS, et al. HSV-1 Infection Induces a Downstream Shift of Promoter-Proximal Pausing for Host Genes. J Virol. 2023;97(5):e0038123.

40. Heinz S, Benner C, Spann N, Bertolino E, Lin YC, Laslo P, et al. Simple combinations of lineage-determining transcription factors prime cis-regulatory elements required for macrophage and B cell identities. Mol Cell. 2010;38(4):576-89.

41. Barski A, Cuddapah S, Cui K, Roh T-Y, Schones DE, Wang Z, et al. High-Resolution Profiling of Histone Methylations in the Human Genome. Cell. 2007;129(4):823-37.

42. Shivaswamy S, Bhinge A, Zhao Y, Jones S, Hirst M, Iyer VR. Dynamic remodeling of individual nucleosomes across a eukaryotic genome in response to transcriptional perturbation. PLoS Biol. 2008;6(3):e65.

43. Tirosh I, Barkai N. Two strategies for gene regulation by promoter nucleosomes. Genome Res. 2008;18(7):1084-91.

44. Hartley PD, Madhani HD. Mechanisms that specify promoter nucleosome location and identity. Cell. 2009;137(3):445-58.

45. Greenberg RS, Long HK, Swigut T, Wysocka J. Single Amino Acid Change Underlies Distinct Roles of H2A.Z Subtypes in Human Syndrome. Cell. 2019;178(6):1421-36 e24.

46. Bagchi DN, Battenhouse AM, Park D, Iyer VR. The histone variant H2A.Z in yeast is almost exclusively incorporated into the +1 nucleosome in the direction of transcription. Nucleic Acids Research. 2020;48(1):157-70.

47. Lashgari A, Millau J-F, Jacques P-É, Gaudreau L. Global inhibition of transcription causes an increase in histone H2A.Z incorporation within gene bodies. Nucleic Acids Research. 2017;45(22):12715-22.

48. Wyler E, Menegatti J, Franke V, Kocks C, Boltengagen A, Hennig T, et al. Widespread activation of antisense transcription of the host genome during herpes simplex virus 1 infection. Genome Biology. 2017;18(1):209.

49. Jimeno-González S, Ceballos-Chávez M, Reyes JC. A positioned +1 nucleosome enhances promoter-proximal pausing. Nucleic Acids Research. 2015;43(6):3068-78.

50. Conn KL HM, Schang LM. Linker histones are mobilized during infection with herpes simplex virus type 1. J Virol. 2008;82:8629–46.

51. Conn KL HM, Schang LM. Core histones H2B and H4 are mobilized during infection with herpes simplex virus 1. J Virol. 2011;85:13234–52.

52. Conn KL, Schang LM. Chromatin Dynamics during Lytic Infection with Herpes Simplex Virus 1. Viruses. 2013;5(7):1758-86.

53. Stow ND, Stow EC. Isolation and Characterization of a Herpes Simplex Virus Type 1 Mutant Containing a Deletion within the Gene Encoding the Immediate Early Polypeptide Vmw110. Journal of General Virology. 1986;67(12):2571-85.

54. Post LE, Roizman B. A generalized technique for deletion of specific genes in large genomes: a gene 22 of herpes simplex virus 1 is not essential for growth. Cell. 1981;25(1):227-32.

55. Smith IL, Hardwicke MA, Sandri-Goldin RM. Evidence that the herpes simplex virus immediate early protein ICP27 acts post-transcriptionally during infection to regulate gene expression. Virology. 1992;186(1):74-86.

56. Fenwick ML, Everett RD. Inactivation of the Shutoff Gene (UL41) of Herpes Simplex Virus Types 1 and 2. Journal of General Virology. 1990;71(12):2961-7.

57. Kluge M, Friedel CC. Watchdog - a workflow management system for the distributed analysis of large-scale experimental data. BMC Bioinformatics. 2018;19(1):97.

58. Kluge M, Friedl MS, Menzel AL, Friedel CC. Watchdog 2.0: New developments for reusability, reproducibility, and workflow execution. Gigascience. 2020;9(6).

59. Bonfert T, Kirner E, Csaba G, Zimmer R, Friedel CC. ContextMap 2: fast and accurate context-based RNA-seq mapping. BMC Bioinformatics. 2015;16:122.

60. Li H, Durbin R. Fast and accurate short read alignment with Burrows-Wheeler transform. Bioinformatics. 2009;25(14):1754-60.

61. Danecek P, Bonfield JK, Liddle J, Marshall J, Ohan V, Pollard MO, et al. Twelve years of SAMtools and BCFtools. Gigascience. 2021;10(2).

62. Quinlan AR, Hall IM. BEDTools: a flexible suite of utilities for comparing genomic features. Bioinformatics. 2010;26(6):841-2.

63. R Core Team. R: A Language and Environment for Statistical Computing. Vienna, Austria2022.

64. Hahne F, Ivanek R. Visualizing Genomic Data Using Gviz and Bioconductor. Methods Mol Biol. 2016;1418:335-51.

65. Chirackal Manavalan AP, Pilarova K, Kluge M, Bartholomeeusen K, Rajecky M, Oppelt J, et al. CDK12 controls G1/S progression by regulating RNAPII processivity at core DNA replication genes. EMBO Rep. 2019;20(9):e47592.

66. Benjamini Y HY. Controlling the False Discovery Rate: A Practical and Powerful Approach to Multiple Testing. Journal of the Royal Statistical Society Series B (Methodological). 1995;57(1):289-300.

67. Raudvere U, Kolberg L, Kuzmin I, Arak T, Adler P, Peterson H, et al. g:Profiler: a web server for functional enrichment analysis and conversions of gene lists (2019 update). Nucleic Acids Res. 2019;47(W1):W191-W8.

68. Kolberg L, Raudvere U, Kuzmin I, Vilo J, Peterson H. gprofiler2 -- an R package for gene list functional enrichment analysis and namespace conversion toolset g:Profiler. F1000Res. 2020;9.

69. Quinlan AR, Hall IM. BEDTools: a flexible suite of utilities for comparing genomic features. Bioinformatics. 2010;26(6):841-2.

70. Boyle AP, Guinney J, Crawford GE, Furey TS. F-Seq: a feature density estimator for high-throughput sequence tags. Bioinformatics. 2008;24(21):2537-8.

71. Liao Y, Smyth GK, Shi W. featureCounts: an efficient general purpose program for assigning sequence reads to genomic features. Bioinformatics. 2014;30(7):923-30.

72. Love MI, Huber W, Anders S. Moderated estimation of fold change and dispersion for RNA-seq data with DESeq2. Genome Biol. 2014;15(12):550.

Figures

Fig. 1: HSV-1 infection impacts chromatin accessibility around promoters for the majority of host genes.

(a) Heatmap illustrating the location of differential regions (m- and i-RegC) identified by RegCFinder on the ATAC-seq data for WT, ΔICP0, ΔICP22, ΔICP27, and Δ*vhs* infection in comparison to mock infection. Results are shown for 4,981 (out of 7,649) promoter windows containing at least one statistically significant (adj. p. ≤ 0.01) differential region for at least one virus infection compared to mock. Red and blue colors represent m-RegC (mock>infection) and i-RegC (infection>mock) locations, respectively, within promoter windows. Here, each row of the heatmap shows results for the same input window in different comparisons of virus infection to mock. Colored rectangles on top of the heatmap indicate which virus infection was compared to mock. Black vertical lines in the center of each part of the heatmap indicate the position of the TSS. Hierarchical clustering was performed according to Euclidean distances and Ward's clustering criterion and the cutoff on the hierarchical clustering dendrogram was selected to obtain 14 clusters (marked by colored rectangles between dendrogram and heatmap and numbered from top to bottom as indicated). **(b)** Metagene plot showing the average ATAC-seq profile around the TSS ± 3 kb in mock (red) and WT (blue) infection for cluster 5, an example for pattern (i). For a description of metagene plots, see Materials and Methods. The colored bands below the metagene curves in each panel indicate the percentage of genes having an i- or m-RegC (blue or red, respectively) at that position. **(c)** Read coverage in a ±3.6 kb window around the TSS in ATAC-seq data of mock (red) and WT (blue) infection for an example gene (FBXO28) with pattern (i). Read coverage was normalized to total number of mapped reads for each sample and averaged between replicates. The TSS is indicated by a short vertical line below the read coverage track for mock infection. Gene annotation is indicated at the top. Boxes represent exons, lines represent introns, and direction of transcription is indicated by arrowheads. Below the read coverage track for WT infection, m-RegC (red bars) and i-RegC (blue bars) are shown for the

comparison of WT vs. mock infection. **(d)** Metagene plot as in **(b)** for cluster 7, the most pronounced case of pattern (ii). **(e)** Read coverage plot as in **(c)** for an example gene (ARHGAP1) with pattern (ii). Here, the promoter window also contains the TSS of the ZNF408 gene on the opposite strand and the accessible chromatin region extends upstream of the ARHGAP1 TSS, i.e. downstream of the ZNF408 TSS. **(f,g)** Metagene plots as in **(b)** for **(f)** cluster 13, which exhibits pattern (iii), and **(g)** cluster 8, one of two clusters exhibiting the combined (i)+(ii) pattern.

Fig. 2: Changes in chromatin accessibility at promoters are mostly independent of dOCR induction and linked to transcription.

(a) Bar plots showing the percentage of promoter regions for each cluster overlapping with dOCRs downstream of the 1,296 genes for which we previously showed consistent dOCR induction across different HSV-1 strains (30). dOCR regions in mock, WT (± PAA treatment) and null mutant infection were calculated as previous described (30) (see Materials and Methods for further details) and the overlaps of promoter windows to dOCR regions originating from an upstream gene were determined for each cluster. WT (± PAA treatment) and null mutant infection are ordered according to the overall extent of dOCR induction. Only few clusters (12-14) showed some enrichment for dOCRs from upstream genes, which was abolished in ΔICP22 infection. **(b-d)** Metagene curves showing average ATAC-seq profiles in promoter windows for mock (red), WT (blue) and WT+PAA (green) infection for clusters 5 **(b)**, 7 **(c),** and 13 **(d)**. See Materials and Methods for a detailed description of metagene plots. PAA treatment reduces the downstream and upstream broadening for patterns (i) (example cluster in **b**) and (ii) (example cluster in **c**), respectively, but enhances pattern (iii) (in **d**), which is enriched for dOCR induction from upstream genes. **(e,f)** Boxplots showing the distribution of **(e)** gene expression (FPKM) values and **(f)** log2 DSR:UAR ratios in

chromatin-associated RNA in mock (red) and 8 h p.i. WT (blue) HSV-1 infection for all clusters (grouped by pattern, cluster numbers are shown below each boxplot) and remaining genes without significant chromatin accessibility changes (NA group). DSR was calculated as the expression (FPKM) in chromatin-associated RNA for the region downstream of the TSS in sense direction and UAR as the expression (FPKM) in the upstream region in antisense direction. P-values for Wilcoxon rank sum tests comparing values in mock infection for each cluster/group against all other analyzed genes are indicated below cluster numbers and were corrected for multiple testing using the Bonferroni method.

Fig. 3: Changes in chromatin accessibility at promoters are detectable as early as 4 h p.i. **(a)** Heatmap showing the log2 fold-changes determined with DEXSeq on the ATAC-seq time-course data (1, 2, 4, 6 and 8 h p.i. WT infection compared to mock infection) for statistically significant differential regions (m- and i-RegC) identified by RegCFinder. For comparison, log2 fold-changes for the WT vs. mock comparison from **Fig 1a** are also shown. Each row represents the results for one of the input windows included in **Fig. 1a**. Colored rectangles on top indicate the time-point of infection or whether the original WT vs. mock comparison is shown. Statistically significant differential regions are colored according to the log2 fold-change determined by DEXSeq. Here, the color scale is continuous between -1 and 1 and all log2 fold-changes >1 are colored the same red and all log2 fold-changes <1 the same blue. Promoter windows are ordered as in **Fig. 1a** and clusters are annotated as colored and numbered rectangles on the left. **(b)** Number (no.) of statistically significant differential regions (m- and i-RegC) and number of genes with at least one statistically significant differential region identified for each time-point of infection in the ATAC-seq time-course data. **(c)** Metagene plot of ATAC-seq profiles in mock infection (red) and all time-points of infection (blue shades) from the ATAC-seq time-course experiment for example cluster 5 (pattern (i)). The colored bands below the metagene curves in each panel indicate the

percentage of genes having an i- or m-RegC (blue or red, respectively) at that position in the comparison of 8 h p.i. to mock infection from the time-course experiment. Metagene plots for all clusters are shown in **Sup. Fig. 20**.

Fig. 4: HSV-1 infection and depletion of Pol II from human genes lead to a downstream shift of H2A.Z-containing +1 nucleosomes.

(a) Heatmap showing the location for differential regions (m- and i-RegC) identified in the WT vs. mock comparison on the ATAC-seq (left half, identical to left-most part of **Fig. 1a**) and H2A.Z ChIPmentation data (right half) for the promoter windows included in **Fig. 1a.** Differential regions with mock>infection (m-RegC) are marked in red, differential regions with infection>mock (i-RegC) in blue. The order of promoter windows is the same as in **Fig. 1a** and clusters are indicated by colored and numbered rectangles on the left. **(b,c)** Read coverage in a ±3.6 kb window around the TSS in H2A.Z ChIPmentation data for mock (red) and WT (blue) infection for example genes with **(b)** pattern (i) (FBXO28) and **(c)** pattern (ii) (ARHGAP1). For descriptions of read coverage plots see caption to **Fig. 1**. **(d-g)** Metagene plots of H2A.Z profiles for mock and WT infection **(d,e)** and untreated and α-amanitin-treated HCT116 cells **(f,g)** for clusters 5 (pattern (i), **d,f**) and 7 (pattern (ii), **e,g**). Metagene plots for other clusters can be found in **Sup. Fig. 23** and **25**, respectively. The colored bands below the metagene curves in each panel indicate the percentage of genes having m- or i-RegC at that position. For **(f,g)**, m-RegC (green) are differential regions with relative read coverage higher in untreated cells and i-RegC (violet) differential regions with relative read coverage higher upon α-amanitin-treatment.

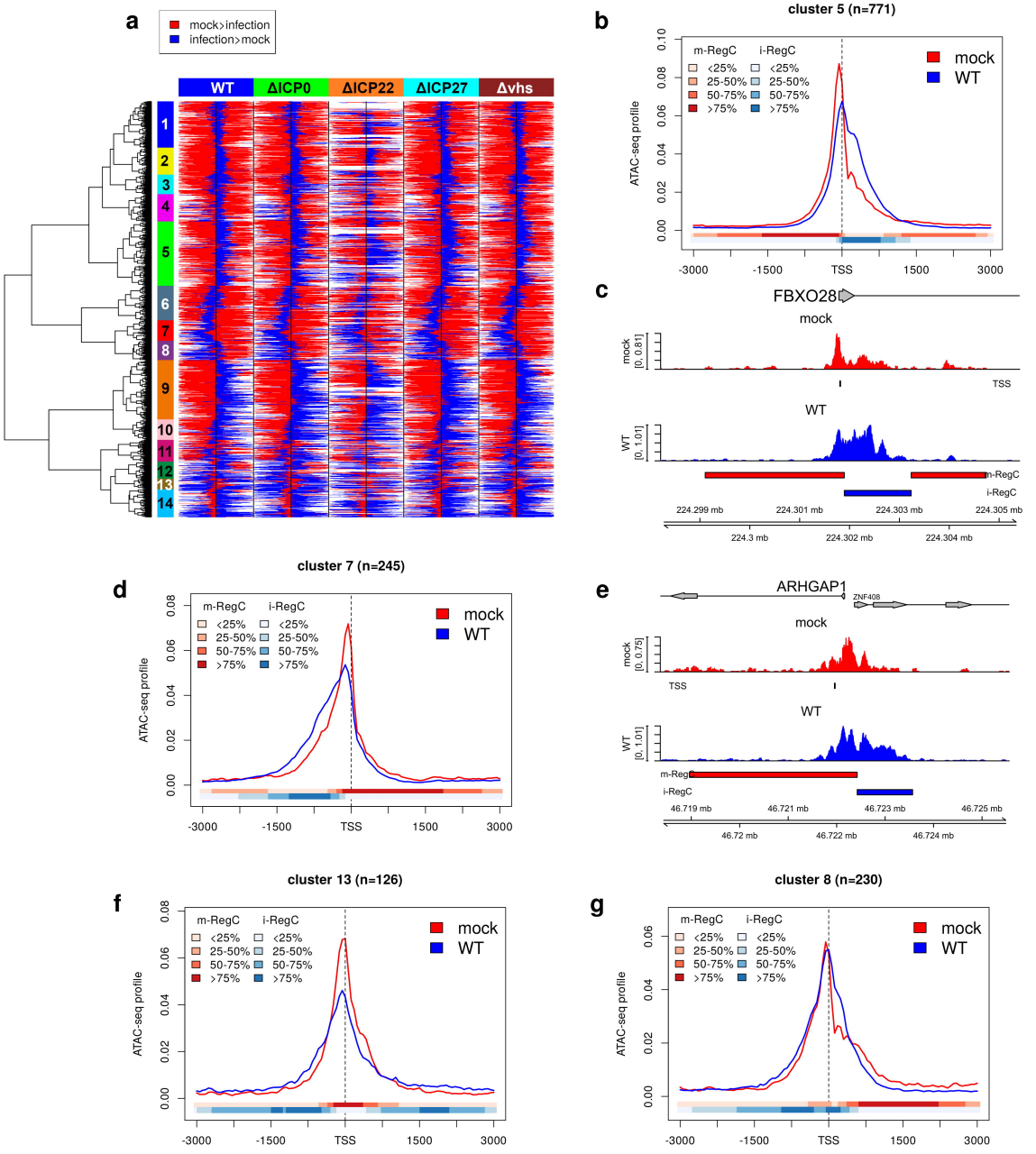
a
mock>infection
infection>mock
WT
ΔICP0
ΔICP22
ΔICP27
Δvhs
1
2
3
4
5
6
7
8
9
10
11
12
13
14
b
cluster 5 (n=771)
m-RegC
i-RegC
<25%
25-50%
50-75%
>75%
mock
WT
ATAC-seq profile
-3000
-1500
TSS
1500
3000
c
FBXO28
mock
WT
TSS
m-RegC
i-RegC
224.299 mb
224.301 mb
224.303 mb
224.305 mb
224.3 mb
224.302 mb
224.304 mb
d
cluster 7 (n=245)
e
ARHGAP1
ZNF408
46.719 mb
46.721 mb
46.723 mb
46.725 mb
46.72 mb
46.722 mb
46.724 mb
f
cluster 13 (n=126)
g
cluster 8 (n=230)

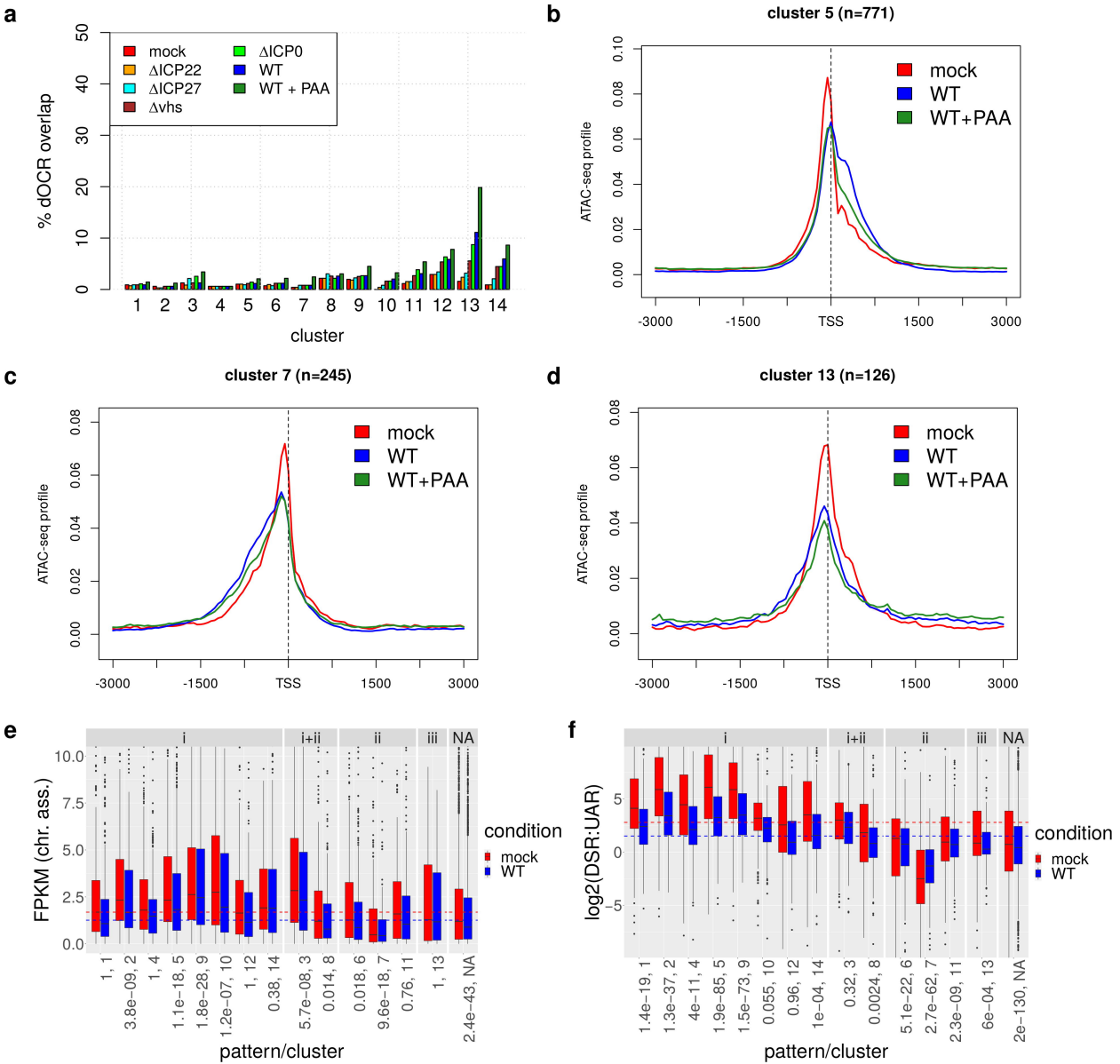
a
% dOCR overlap
cluster
mock
ΔICP22
ΔICP27
Δvhs
ΔICP0
WT
WT + PAA
b
cluster 5 (n=771)
ATAC-seq profile
mock
WT
WT+PAA
TSS
c
cluster 7 (n=245)
d
cluster 13 (n=126)
e
FPKM (chr. ass.)
condition
pattern/cluster
f
log2(DSR:UAR)

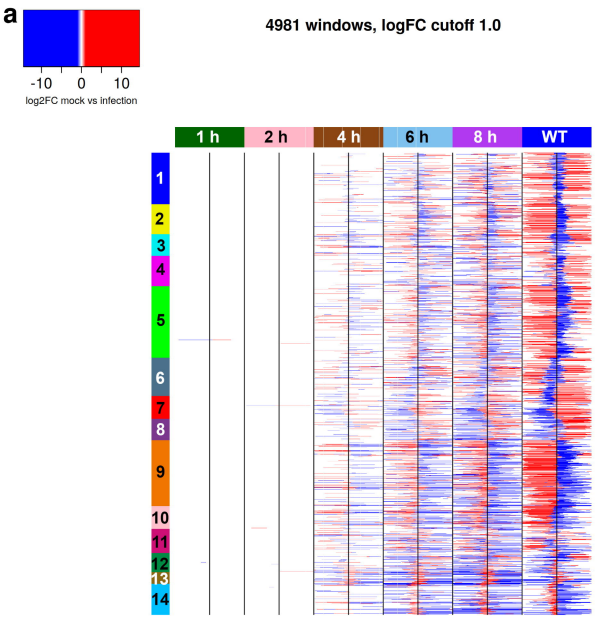
a
-10
0
10
log2FC mock vs infection
4981 windows, logFC cutoff 1.0
1 h
2 h
4 h
6 h
8 h
WT
1
2
3
4
5
6
7
8
9
10
11
12
13
14

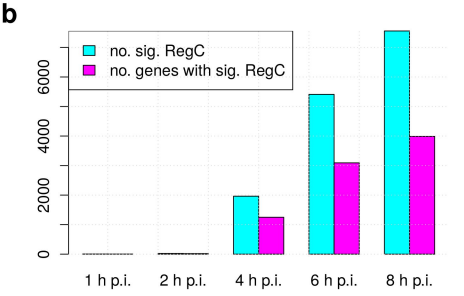
b
no. sig. RegC
no. genes with sig. RegC
0
2000
4000
6000
1 h p.i.
2 h p.i.
4 h p.i.
6 h p.i.
8 h p.i.

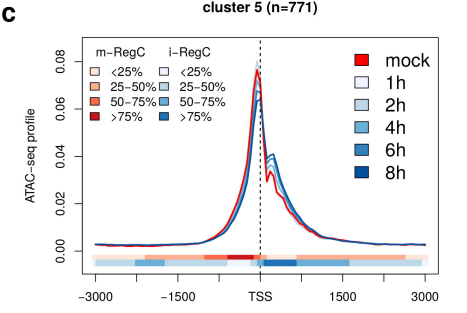
c
cluster 5 (n=771)
m−RegC
i−RegC
<25%
25−50%
50−75%
>75%
mock
1h
2h
4h
6h
8h
ATAC−seq profile
0.00
0.02
0.04
0.06
0.08
−3000
−1500
TSS
1500
3000

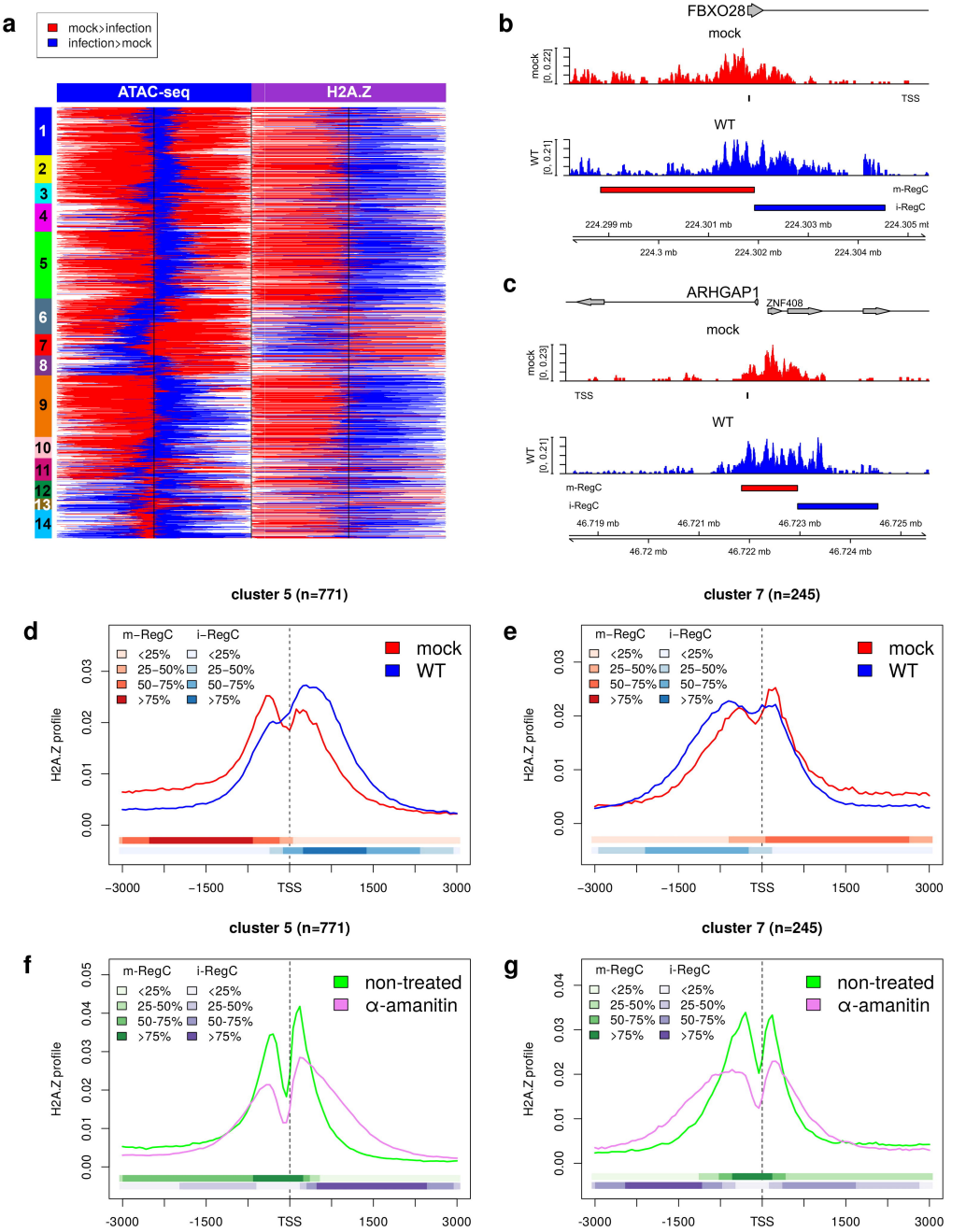
a
mock>infection
infection>mock
ATAC-seq
H2A.Z
1
2
3
4
5
6
7
8
9
10
11
12
13
14
b
FBXO28
mock
mock
[0, 0.22]
TSS
WT
WT
[0, 0.21]
m-RegC
i-RegC
224.299 mb
224.301 mb
224.303 mb
224.305 mb
224.3 mb
224.302 mb
224.304 mb
c
ARHGAP1
ZNF408
mock
mock
[0, 0.23]
TSS
WT
WT
[0, 0.21]
m-RegC
i-RegC
46.719 mb
46.721 mb
46.723 mb
46.725 mb
46.72 mb
46.722 mb
46.724 mb
cluster 5 (n=771)
cluster 7 (n=245)
d
e
m-RegC
i-RegC
<25%
25–50%
50–75%
>75%
mock
WT
H2A.Z profile
0.00
0.01
0.02
0.03
−3000
−1500
TSS
1500
3000
cluster 5 (n=771)
cluster 7 (n=245)
f
g
non-treated
α-amanitin
H2A.Z profile
0.00
0.01
0.02
0.03
0.04
0.05
-3000
-1500
TSS
1500
3000